AFRL-RZ-WP-TR-2010-2119

A GUIDE TO ELECTRICAL INSULATION DESIGN IN AEROSPACE VEHICLES FOR A BROAD RANGE OF ENVIRONMENTAL PARAMETER SPACE

Daniel Schweickart, John Horwath, Lawrence Walko, Lynn Hatfield, and Hermann Krompholz

Energy and Power Systems Branch
Energy/Power/Thermal Division

MARCH 2010
Final Report

AIR FORCE RESEARCH LABORATORY
PROPULSION DIRECTORATE
WRIGHT-PATTERSON AIR FORCE BASE, OH 45433-7251
AIR FORCE MATERIEL COMMAND
UNITED STATES AIR FORCE

NOTICE AND SIGNATURE PAGE

This report was cleared for public release by the USAF 88th Air Base Wing (88 ABW) Public Affairs (AFRL/PA) Office and is available to the general public, including foreign nationals. Copies may be obtained from the Defense Technical Information Center (DTIC) (http://www.dtic.mil).

AFRL-RZ-WP-TR-2010-2119 HAS BEEN REVIEWED AND IS APPROVED FOR PUBLICATION IN ACCORDANCE WITH THE ASSIGNED DISTRIBUTION STATEMENT.

*//Signature//
DANIEL SCHWEICKART
Energy and Power Systems Branch
Energy/Power/Thermal Division

//Signature//
RUSSELL SPYKER, Deputy Chief
Energy and Power Systems Branch
Energy/Power/Thermal Division
Propulsion Directorate

REPORT DOCUMENTATION PAGE

Form Approved
OMB No. 0704-0188

1. REPORT DATE *(DD-MM-YY)*	2. REPORT TYPE	3. DATES COVERED *(From - To)*
March 2010	Final	15 December 2001 – 15 December 2009

4. TITLE AND SUBTITLE
A GUIDE TO ELECTRICAL INSULATION DESIGN IN AEROSPACE VEHICLES FOR A BROAD RANGE OF ENVIRONMENTAL PARAMETER SPACE

5a. CONTRACT NUMBER
In-house

5b. GRANT NUMBER

5c. PROGRAM ELEMENT NUMBER
62203F

6. AUTHOR(S)
Daniel Schweickart, John Horwath, Lawrence Walko, Lynn Hatfield, and Hermann Krompholz

5d. PROJECT NUMBER
3145

5e. TASK NUMBER
32

5f. WORK UNIT NUMBER
314532Z7

7. PERFORMING ORGANIZATION NAME(S) AND ADDRESS(ES)
Energy and Power Systems Branch (AFRL/RZPE)
Energy/Power/Thermal Division, Air Force Research Laboratory
Propulsion Directorate
Wright-Patterson Air Force Base, OH 45433-7251
Air Force Materiel Command, United States Air Force

8. PERFORMING ORGANIZATION REPORT NUMBER
AFRL-RZ-WP-TR-2010-2119

9. SPONSORING/MONITORING AGENCY NAME(S) AND ADDRESS(ES)
Air Force Research Laboratory
Propulsion Directorate
Wright-Patterson Air Force Base, OH 45433-7251
Air Force Materiel Command
United States Air Force

10. SPONSORING/MONITORING AGENCY ACRONYM(S)
AFRL/RZPE

11. SPONSORING/MONITORING AGENCY REPORT NUMBER(S)
AFRL-RZ-WP-TR-2010-2119

12. DISTRIBUTION/AVAILABILITY STATEMENT
Approved for public release; distribution unlimited.

13. SUPPLEMENTARY NOTES
PAO Case Number: 88ABW-2010-1711, Clearance Date: 30 Mar 2010. Report contains color.

14. ABSTRACT
As mission scenarios expand and flight profiles change, both military and commercial aerospace vehicles will be required to operate in a broader range of environments than current flight vehicles. This implies the need for increased reliability across a wide range of environmental conditions, i.e., environmental parameter space. A critical element to the overall operational capability of the vehicle is the reliability of the electrical systems onboard. In the case of electrical systems insulation, both reliability and lifetime can depend on addressing the relevant environmental issues in the design phase, to minimize or eliminate the degrading effects of corona or gas volume breakdown that can lead to insulation system failures. The information contained herein is a technology review of corona and discharge research, including technologies specific to the characterization of gaseous insulation breakdown in geometries of high electrical field stress. The report attempts to better define the parameter space for gas environments applicable to aerospace power in advanced military flight platforms, with some applicability to commercial aircraft and spacecraft, as well.

15. SUBJECT TERMS
electrical insulation systems, breakdown, reliability, environmental parameter space, pressure

16. SECURITY CLASSIFICATION OF:			17. LIMITATION OF ABSTRACT:	18. NUMBER OF PAGES	19a. NAME OF RESPONSIBLE PERSON (Monitor)
a. REPORT	b. ABSTRACT	c. THIS PAGE			Daniel Schweickart
Unclassified	Unclassified	Unclassified	SAR	48	19b. TELEPHONE NUMBER *(Include Area Code)* N/A

Standard Form 298 (Rev. 8-98)
Prescribed by ANSI Std. Z39-18

TABLE OF CONTENTS

LIST OF FIGURES

LIST OF TABLES

PREFACE

This report contains information acquired during the execution of an internal program entitled, "The Effects of Emissions from and Susceptibility to Electromagnetic Fields, Corona, and Discharges on Advanced Aerospace Power Systems," and through collaborations with Professors Hatfield and Krompholz (Texas Tech University), as well as Mr. Walko (who initiated the program prior to his retirement from AFRL/RZP). The information contained herein is a technology review of corona and discharge research, including technologies specific to the characterization of gaseous insulation breakdown in geometries of high electrical field stress. The report attempts to better define the parameter space for gas environments applicable to aerospace power in advanced military flight platforms, with some applicability to commercial aircraft and spacecraft, as well. Breakdown characteristics as a function of electric field stress, gas density and applied frequency are documented. Section 1 provides a brief introduction to the background for this work. Section 2 defines the objectives behind the literature review that was performed. Section 3 considers breakdown in uniform dc fields, Section 4 deals with unipolar pulsed discharges, Section 5 considers alternating current (ac) breakdown, and Section 6 presents a summary. Section 7 contains the references to the report.

1. INTRODUCTION

As mission scenarios expand and flight profiles change, both military and commercial aerospace vehicles will be required to operate in a broader range of environments than current flight vehicles. This implies the need for increased reliability across a wide range of environmental conditions, i.e., environmental parameter space. A critical element to the overall operational capability of the vehicle is the reliability of the electrical systems onboard. In the case of electrical systems insulation, both reliability and lifetime can depend on addressing the relevant environmental issues in the design phase, to minimize or eliminate the degrading effects of corona or gas volume breakdown that can lead to insulation system failures.

Fuel efficiency and weight considerations are just a couple of the drivers for increased electrical power utilization on both commercial and military aircraft in the development. The airborne electrical power system loading is increasing in many subsystems, for example, housekeeping power (avionics displays and in-flight entertainment), flight control (electrical actuation), and special high power (dedicated to weapons systems). For power system applications in high altitude flight vehicles (manned and unmanned), the potential environmental parameter space is much larger than that experienced by legacy flight vehicles. By their very nature, special high power subsystems produce and experience high-level electromagnetic fields, currents, and voltages within the interior of airborne platforms. These internally generated fields, currents, and voltages will be a part of its operational environment, and the complete system must be designed to operate properly at the generated field, current, and voltage levels.

2. LITERATURE REVIEW

As was stated in the Introduction, new developments in weapons technology for aircraft/spacecraft require the application of various high-voltage devices exposed to atmospheric conditions. This report has two objectives; one, to present the known limits for the applicability of high voltage with an ambient gas as main insulation and two, to determine what additional information is needed to perform an adequate insulation design. These objectives in more detail are:

1. Define high-voltage breakdown thresholds for altitudes from sea level to 100,000 ft, for a variety of conditions, such as dc voltages, pulsed voltages (pulse durations down to the nanosecond regime), repetition-rated pulsed voltages, sinusiodal ac conditions (mainly for power conditioning, for frequencies below the MHz regime with emphasis on the frequency domain below 100 kHz). Supplementary information is given for the microwave regime and includes volume breakdown as well as surface flashover for frequencies in the GHz regime, including continuous wave (CW), pulsed, and repetition-rated conditions.

2. Define areas of breakdown phenomenology, in which the present knowledge is not sufficient to provide reliable data, and in which additional basic research is required.

A literature search was performed to gather information to address these objectives. About 90 percent of the relevant information is found in monographs on gas discharges and

related phenomena; journal and conference papers supplement this information. It should be noted that during the last couple of decades (approximately 1990 to the present) not much new quantitative information has been published in the field of gas discharge fundamentals.

3. BREAKDOWN IN UNIFORM FIELDS

3.1 Townsend-Paschen Theory

The classical and historically first estimation of the breakdown voltage is the Townsend-Paschen theory, Paschen (1889) [1], de la Rue and Mueller (1880) [2], Hurst (1906) [3], Townsend (1900) [4], (1901) [5], (1902) [6], see also Meek and Craggs (1978) [7], Nasser (1971) [8]. This model is applicable for dc gaseous breakdown, for pressures usually between several millitorr to several atmospheres, and gap distances of millimeters to several centimeters, and for homogeneous fields. The basics of this model are the following:

The electron density in a supercritical (i.e., amplifying) field evolves according to

$$n_e(x) = n_e(0)\exp(\alpha x) \ , \tag{1}$$

where $n_e(0)$ is the starting electron density, e.g., at the cathode, x is the coordinate along the gap starting at the cathode, and α is the net number of electron-ion-pairs created by collisions per unit distance (number of ionizing collisions minus the number of recombination-collisions, such as attachment).

The fact that ionization requires a minimum impact energy $E_i = W_i/e$, results in a minimum free path between ionizations of $\lambda_i = E_i/E$, where E is the applied electric field. From elementary gas theory, it follows that the probability of a collision with free path > x is exp(-x/λ), where λ is the mean free path (mainly determined by elastic collisions). From geometric considerations it follows that $v_{av}/\lambda = v_D/\lambda_E$ (v_{av} average velocity, v_D drift velocity, i.e., velocity component parallel to the applied field, λ_E mean free path parallel to field). Then the ionization coefficient is

$$\alpha = n_E \exp(-\lambda_i/\lambda) = \frac{1}{\lambda_E}\exp(-\frac{E_i}{E_\lambda}) \ , \tag{2}$$

where n_E is the number of collisions per unit length parallel to E, $1/\lambda_E = n_E$, and E_λ is energy gained between collisions in the direction of the field.

Since both λ and λ_i are inversely proportional to the pressure p, it follows that

$$\alpha = Ap\exp(-Bp/E) \tag{3}$$

which is one of the important basic scaling laws for Paschen breakdown. A and B are physical constants (related to elastic and inelastic collisions between the free electrons and molecules).

Modeling the transition from electron avalanches to a self-sustaining discharge requires a feedback mechanism, which forces the electron density to approach infinity during a finite time. In reality, the corresponding current is limited by the applied voltage and the circuit impedance. The most important feedback mechanism is creation of free electrons at the cathode either by ions or by radiation. In standard descriptions, an electron number n_0 is created at the cathode by external means, such as external radiation. The total number of electrons leaving the cathode is

$$n_0' = n_0 + \gamma_i (n - n_0') \ , \tag{4}$$

where n is the total number of electrons produced in the gap, and γ_i is the coefficient relating the number of newly released electrons to the number of electrons in the gap. The form of this relationship holds for most of the possible feedback mechanisms (positive ions from gap, positive ions from anode, radiation).
Solving this equation for n_0' results in

$$n_0' = \frac{n_0 + \gamma_i n}{1 + \gamma_i} \ . \tag{5}$$

Since $n = n_0' \exp(\alpha d)$ it follows furthermore that

$$n = \frac{\exp(\alpha d)}{1 - \gamma_i [\exp(\alpha d) - 1]} \ . \tag{6}$$

According to this equation, breakdown occurs if the denominator approaches zero, or

$$\gamma_i (e^{\alpha d} - 1) = 1 \ . \tag{7}$$

Since $\alpha/p = f(E/p) = f(V_B/(pd))$, it finally follows for the functional dependence of the breakdown voltage V_B

$$V_B = f(pd) \tag{8}$$

as general relationship, or, within the framework of the equations above,

$$V_B = \frac{Bpd}{\ln\{\frac{Apd}{\ln(1 + \frac{1}{\gamma_i})}\}} \ . \tag{9}$$

The characteristic behavior of this relationship is depicted in Figure 1. V_B versus pd has a minimum at

$$pd = (pd)_{\min} = \frac{e}{A} \ln(\frac{1}{\gamma_i} + 1) \ , \tag{10}$$

with a minimum voltage of

$$V_B = V_{B\min} = e \frac{B}{A} \ln(\frac{1}{\gamma_i} + 1) \ . \tag{11}$$

V_B approaches infinity at $pd=(pd)_{min}/e$.

As a visual aid to the characteristic shape of the Paschen curve, Figure 1 provides normalized Paschen curves from equation 1. Here, vertical lines denote (pd)min/e for each value of γ.

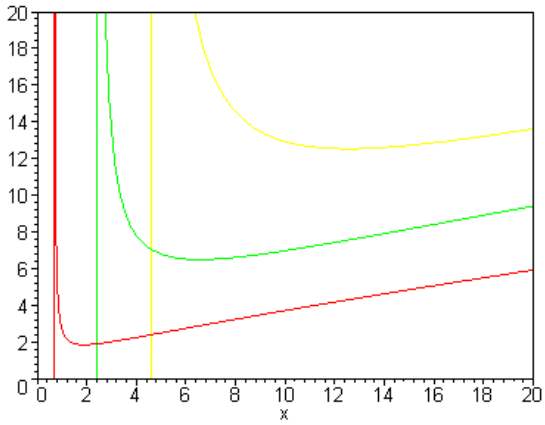

Figure 1. Normalized Paschen-curves According to Equation (1), AV_B/B (y-axis) versus
Apd (x-axis) for γ=0.01 (Upper), 0.1 (Middle), 1 (Lower Curve).

The Townsend-Paschen model describes only collisional processes in the gas, and does not discuss the influence of space charges associated with the developing avalanche. For realistic cases, any developing avalanche reaches conditions, in which the space charge density gets high enough to alter the local value of the electric field and alters the amplification parameters. Usually, the Townsend-Paschen theory is considered to represent an ideal limiting case with an infinite duration of the current rise, in contrast to the real case, in which space charges dominate and a transition to the streamer mechanism takes place, see below. Transitions from Paschen to streamer discharge are described in numerous publications, such as Novak and Bartnikas (1987) [9], Pedersen (1989) [10], Kunhardt (1990) [11], Kunhardt and Byszewski (1980) [12].

3.2 Experimental dc Breakdown Voltages

The simple theory described in the previous section assumes that the collision cross sections are independent of the electron energy, which is of course not the case in reality. Solving the transport equations with real cross sections yields breakdown voltage versus pd curves in close agreement with measured curves (e.g., one of the earliest comparisons of calculated and measured curves by Hurst (1906) [3]; comparison of different authors by Dutton et al., (1961) [13] and Meek and Craggs (1978) [7], see Figure 2: This figure is a reproduction of Figure 6.1 in Meek and Craggs. The γ value, which describes the generation of secondary electrons and the feedback mechanism leading to breakdown, is a function of not only E/p, but also a function of the electrode material. No substantial dependences of these processes on E/p and the electrode material have been found, however, and statements on electrode materials are often omitted. Most measurements

reported in the literature claim an absolute accuracy on the order of a fraction of a percent to about 1 percent.

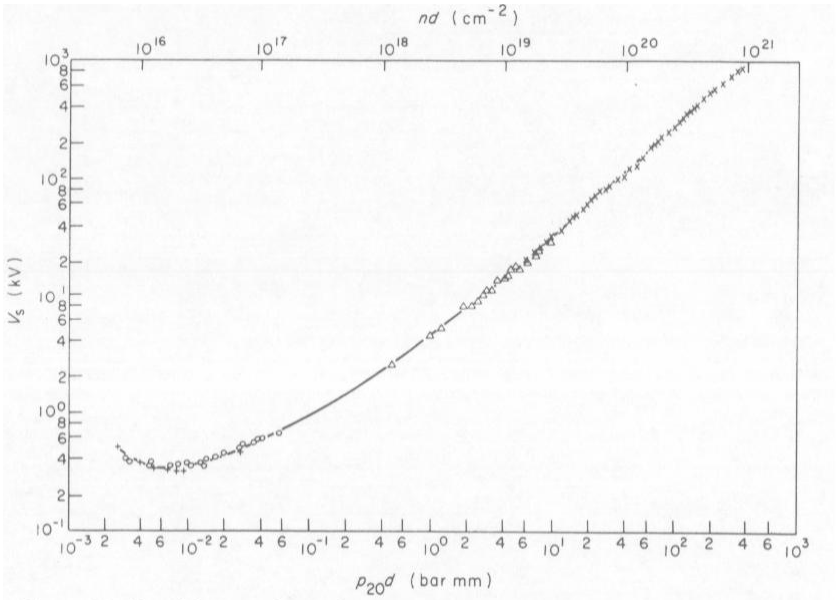

Figure 2. Breakdown voltages in atmospheric air, comparing different national standards and measured values from different authors

For air at atmospheric pressure for uniform fields, the breakdown voltage in kV (expressed as V_B /kV) is

$$V_B \big/ kV = 24.4\rho d + 6.53\sqrt{\rho d} \quad , \tag{12}$$

where d is in cm (for 0.01cm ≤ d ≤ 20 cm), and

$$\rho = \frac{p}{1013 mbar} \frac{293K}{T/°C + 273K}, \tag{13}$$

which has been gained from averaging several experimental results, Allen (2000) [14]. It has accuracy within 1 percent. Further factors influencing the breakdown voltage include gap distance, pressure, electrode geometry (radius of curvature), electrode material, and contaminations, such as humidity, dust. These factors are discussed next.

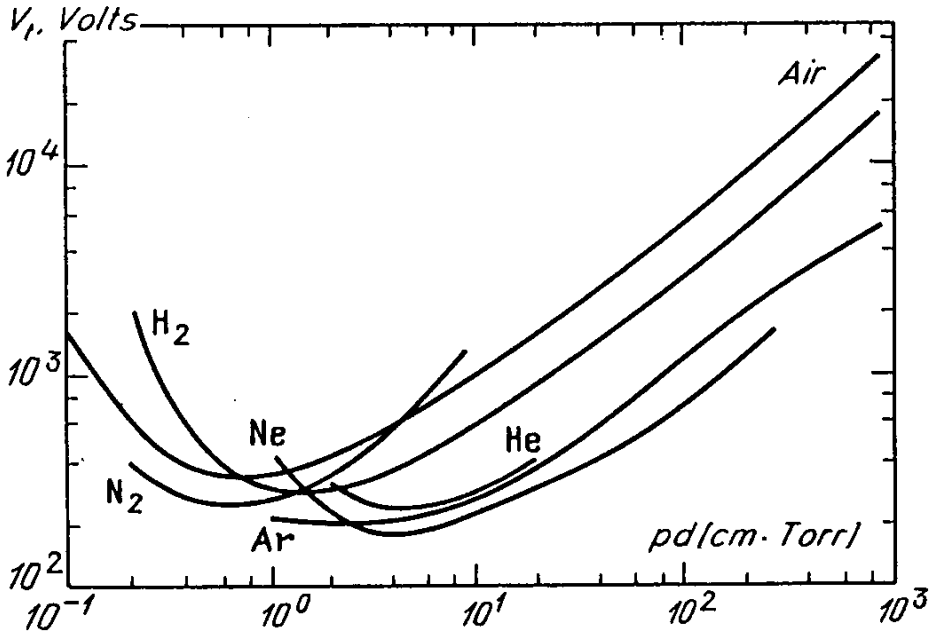

Figure 3. Experimental Paschen curves, comparison of different gases

Paschen curves for various gases are shown in Figure 3 (based on data from Chapter 6 of Meek (1978) [7] and Brown (1966) [74]). Basic measurement techniques to obtain Paschen curves reproducibly and reliably are described in Hanlon (1974) [15]. Temperature dependences, where aside from the reduction in pressure, thermionic emission and thermal ionization are relevant features, have been measured by George (1974) [16]. Practical situations at high temperature often involve flowing boundary layers with temperature and density gradients over small distances, for which empirical data are missing. For homogeneous situations, the validity of Paschen's law has been confirmed for temperatures of up to 1100° C by Powell (1972) [17]. Reduction of the breakdown voltage with increasing temperature for rod-plane gaps, for lightning, switching and power frequency voltages, with technical applications and general scaling laws in mind, have been reported by Allen (2000) [14]. Hiziroglu (2000) [18] describes measured breakdown voltages for sphere-sphere and sphere plane geometries with deviations from theoretical values based on α/p measurements by Geballe (1952) [19] which are in the 1 to 2 percent range for gap distances of 20 to 100 mm for atmospheric pressure in air.

3.2.1 Limits

If pd < 10^{-3} torr cm, no collisions occur in the gap, and the only possible discharge mechanism is a pure vacuum discharge (field emission and various amplification processes). There is a smooth transition between Paschen and vacuum discharge, with the consequence that real breakdown curves are not as steep as idealized ones. Breakdown below the Paschen minimum is characterized by competing processes: vacuum breakdown dependent on the properties of the electrode surface, surface breakdown along the insulator

(either on the vacuum side or on the atmospheric side), and Paschen-type breakdown in the gas. (Compare with Schoenhuber (1969) [20], with an estimate on the limits for the breakdown voltage as a function of the gap distance with pressure as a parameter, with the four types of breakdown distinguished. This paper is very useful for designing high-voltage systems operating in low pressure environment.)

Hackam (1974) [21] describes measurements of the breakdown voltage for the pressure range $5x10^{-7}$ to 10^{-2} torr in air. Influences of the gas vanish for $p < 10^{-5}$ torr. In the region around 10^{-4} torr, the breakdown voltage has a maximum, and it makes a transition to the standard Paschen breakdown voltage for pressures $> 5x10^{-2}$ torr (see Figure 4 from Hackam (1974) [21]). The maximum is attributed to an increase of the work function due to gas coverage.

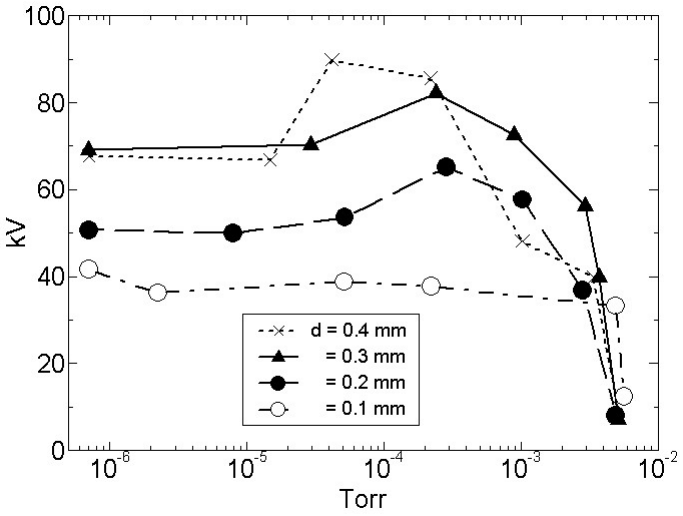

Figure 4. Breakdown voltage in kV versus pressure in air for various gap length with positive point 4-mm rod with 30° cone tapering), and negative plane electrodes

Also, ion-ionization is expected to play a role in the transition region from Paschen to vacuum discharge. A large increase of the secondary ionization coefficient by ions hitting the cathode is shown by Bhasavanich (1977) [22], in model calculations, and compared with experimental data. Furthermore, at low pressure, electron loss due to diffusion seems to be important. Lisovskiy (2000) [23] models these electrons escape losses and derives a modified breakdown law, where the breakdown voltage depends not only on pd, but also on the ratio of gap length and discharge vessel diameter as well. His results agree well with experimental data for pd ranges on the order of 0.1 to 10 Torr cm (see Figure 5).

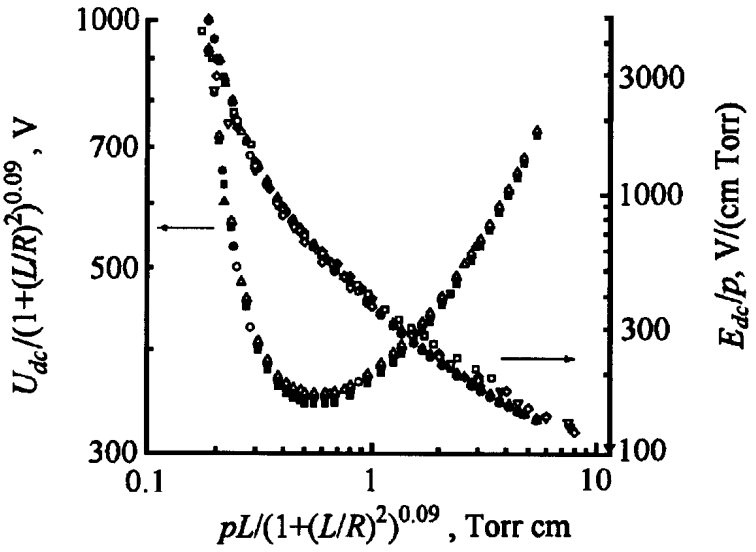

Figure 5. Dependence of breakdown voltage U_{dc} and breakdown field E_{dc}/p on pL in air with discharge tube radius 3.15 cm and different gaps\from 0.5 to 10 cm (theoretical), and comparison with measured data

For large pd values, the influence of space charges (ions left behind with much smaller mobility than electrons) increases with increasing gap distance. Also, field emission at high pressure and moderate gap distance (Watson (1969) [24]) starts at an electric field at the cathode of several 10^5 V/cm. As a consequence, the breakdown voltage deviates from the Paschen law. It gets lower with decreasing gap distance at constant pd. Also for high pressure, statistical variations of the breakdown voltage from discharge to discharge become significant, with a pronounced conditioning effect (increase of breakdown voltage within a series of discharges, as shown in Figure 6 from Goldspink (1968) [25]), especially for large electrode diameters (Goldspink (1968) [25]; Coates (1974) [26]; and see also Meek (1978) pg. 235 [7]). This conditioning effect is important for the reliable operation of spark gaps in self-breakdown mode. Statistical variations can be reduced by roughened electrodes, for examples, where emission or amplification sites lead to breakdown at the lowest possible voltage (Ramirez (1976) [27]).

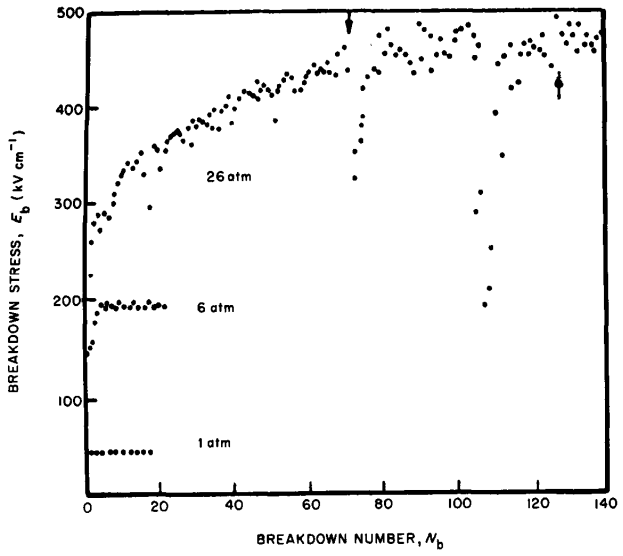

Figure 6. Conditioning effect for high pressure discharges in N_2

Associated with the conditioning effect and the influence of the electrode material are possible amplification mechanisms at very low E/n in the vicinity of a complex surface gas interface. The phenomena in this breakdown regime are not sufficiently characterized to decide which effects are important, which is comparable to the situation for vacuum breakdown; see Cookson (1970) [28] and Cookson (1981) [29].

3.2.2 Electrode Material and Surface Conditions

The electrode material and the electrode surface conditions influence the secondary ionization processes, i.e., creation of photoelectrons, secondary electrons by electron and ion impact, etc. For cases in which electron field emission is decisive (at high fields, or approaching vacuum breakdown conditions), the work function of the material and the work function of material and possible coating (such as adsorbed gas) is the essential parameter. For standard conditions (i.e., Paschen breakdown) differences in the breakdown voltage due to different electrode material are often less than ten percent. See Figure 7 as an example with information from Llewellyn Jones (1939) [30] and from Meek (1978), pg. 233 [7]. Morokuma (1969) [31] varied the surface potential of the electrodes by using nickel coatings of different thickness, and found a linear relationship between change in the work function and breakdown voltage, most pronounced in the region of the minimum of the Paschen curve (approximately 20 V increase in breakdown voltage, for an increase of the work function of 40 mV).

For conditioning effects at high pressure, see Coates (1974) [26] and Ramirez (1975) [27]. An estimation based on modeling of the local electric field distribution due to surface roughness, and the standard streamer breakdown criterion, leads to breakdown voltages decreasing with increasing roughness height, and increasing with increasing sharpness angle; see Mahdy (1998) [32], where a distribution of conical surface structures has been assumed.

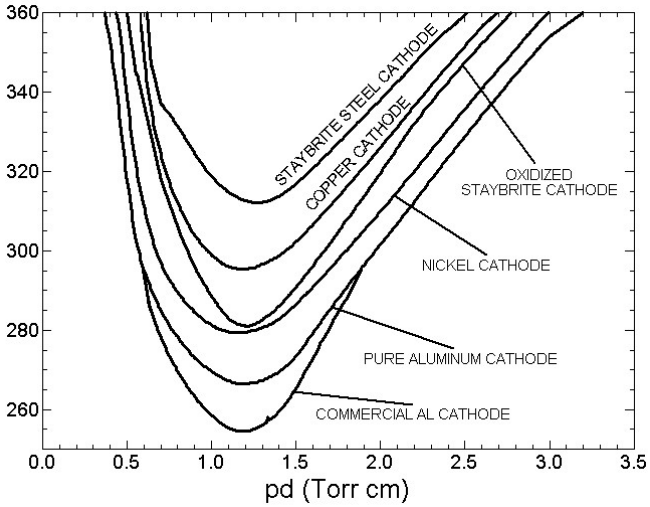

Figure 7. Variation of the breakdown voltage with cathode surface

3.2.3 Electrode Geometry

Many technical applications of high voltage systems or switches use electrode geometries which are by no means flat or would produce homogeneous electric fields. Spatial dependencies of the electric field lead to breakdown criteria, in which the αd dependence has to be replaced by an integral, such as

$$\int_0^d \alpha(x)dx \quad , \tag{14}$$

where α is the ionization coefficient (charge pairs created per unit distance), d the gap width, and x the coordinate along the electric field.

For cases in which the spatial variation of the electric field is small compared to all mean free paths, similarity laws can be applied (Meek, 1978, pg. 588 [7]; See Engel, 1993, pg. 288 [33] for a thorough discussion of similarity laws for most and often all relevant processes in a gas discharge. Estimations of the breakdown voltage for a variety of geometries can be made, where at least one of the electrodes has a macroscopic radius of curvature (either spherical or cylindrical). In gaps with nonuniform field, however, breakdown is often preceded by corona discharge, at a lower voltage.

For practical applications, a corona inception voltage V_i is defined where continuous corona occurs, and V_i is below the breakdown voltage designated as V_s. Also, V_{si} is the breakdown voltage threshold for which a system has to be designed. V_{si} will typically equal V_i if corona occurs, or equal V_s if no detectable corona occurs. (In some systems where corona can be tolerated, V_{si} may be between V_i and V_s.) For uniform field breakdown, Paschen's law states that V_{si} is a function of nd only, where n is gas density and d is distance. This law can cautiously be applied to nonuniform cases, provided that changes in d are accompanied by changes in all other dimensions. This statement can modify Paschen's law such that V_{si} is a function of nr only, where r is the radius of the point with the highest value of the electric field. For gap distances, which are large

compared to radii of curvature, similarity laws can be stated for E_s (which equals V_s/d) in the form E_s/n is a function of nr.

Common empirical relationships for 50 Hz voltages are as follows (Meek (1978) pg. 594 [7]):

$E_s r = 1.27nr + 8.70$, for $14 \le nr \le 100$,

$E_s r = 1.02nr + 37.7$, for $100 \le nr \le 600$ (15)

where E_s is the breakdown field in kV/cm, n the density (air) in units of 10^{18} cm^{-3} (for normal temperature and pressure, n = 25.1) and r is the radius of curvature in cm. These equations are mainly based on measurements with coaxial cylinder gaps of various dimensions, and they agree with results from concentric gaps.

Exact analytical expressions relating the local electric field to the applied voltage can be found for sphere/sphere and cylinder/cylinder arrangements (both with different radii). (They can be found in most introductory textbooks on electromagnetic field theory.) Useful expressions for estimating maximum field strengths at the electrode surfaces are given by the following:

$$E = \frac{V}{\ln(\frac{d + r_e}{r_e}) r_e}$$, for a cylinder of radius r_e at a distance d from a plane (16)

$$E = \frac{V}{(\frac{1}{r_e} - \frac{1}{d}) r_e^{\,2}}$$, for a sphere with radius r_e at a distance d from a plane (17)

$$E / E_{av} = \frac{ah}{r_e} + 1$$, for a semi-ellipsoid with height h and radii of curvature r_e and a (18)

$$E / E_{av} = \frac{h}{r_e} + 2$$, for a cylinder with spherical tip , and (19)

$$E / E_{av} = \frac{h}{2r_e} + 5$$, for a cone with height h and tip radius r_e (20)

(from Mesyats (1989) [34]). In these cases, $E_{av}=V/d$, V applied voltage, d gap width.

Numerous publications deal with the case of a point/plane discharge (corona), where not all of the phenomenological details are completely known.

An example for both theoretical and experimental values of the breakdown voltage as a function of curvature is given in Figure 9 from Pedersen (1989) [10]. The model used here is based on the following breakdown criterion:

$$\int_0^d \alpha(x)dx = K \quad , \tag{21}$$

where the field dependence of α is taken from experimental data for the homogeneous case. Integrating over α with the actual field distribution yields the curves shown in Figure 8 (Full line: rod/plane and sphere/plane gaps. Dashed line: coaxial cylinders. Crosses: experimental data (Pedersen (1989) [10]).

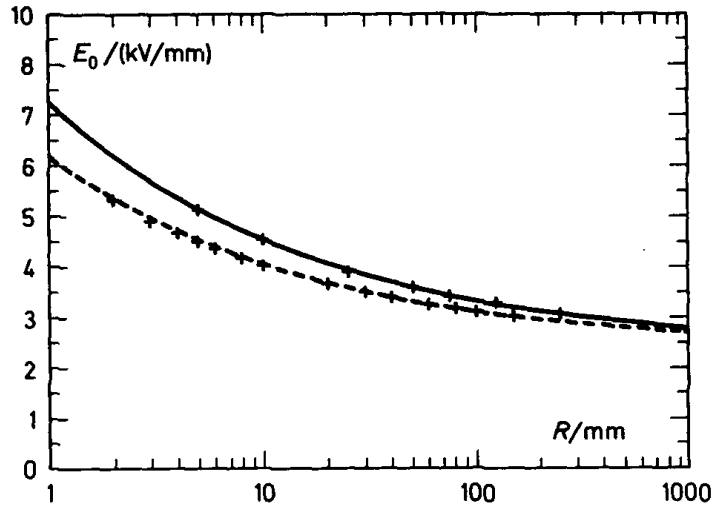

Figure 8. Discharge onset field amplitude E_0 in kV/mm at atmospheric pressure in air as a function of the electrode radius R in mm

Similarity laws for corona development are discussed in Werner (1934) [35] and Hackam (1973) [21]. Figure 9 shows the essential similarity law, E_R versus p_R, see above, applied to corona onset as a function of pressure (Hackam 1973) [21]. In Figure 9 open symbols: Stainless steel electrode with $2R_1$ = 3.96 mm inside coaxial cylinder with 2R = 33.4 mm. Closed symbols: Silver-steel rod with $2R_1$ = 3 mm inside coaxial molybdenum cylinder with 2R = 33 mm.

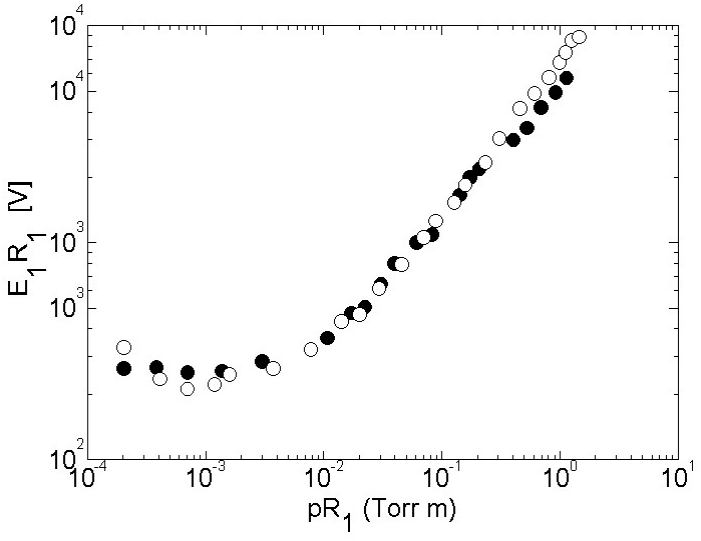

Figure 9. Similarity theorem for corona onset in dry air

Figure 10 shows, as an additional example, corona inception and breakdown voltages for a sphere/sphere system in dry air, as a function of pressure (Raju (1973) [36]). In Figure 10 open triangles are corona and breakdown voltage with inner sphere positive, black triangles breakdown voltage and X's corona inception voltage with inner sphere negative.

Barsch (1992) [37] compares different electrode geometries for power frequency at atmospheric pressure in air, with emphasis on standard rod-rod and rod-plain conductors used in HV arrangements over lengths of several meters, as well as point-plane and sphere-plane geometries, for a gap width between two and 35 cm. Breakdown voltages for all geometries vary between 20 kV at 2 cm to 200 kV at 30 cm. Nishijima (1992) [38] reports about measurements on corona inception and sparkover voltages in electrode arrangements with cylindrical protrusions and hemispherical tips for pressures between 0.2 and 1 bar, compare with Figure 11. In Figure 11 left: negative protrusion with diameter 2 mm at different pressures. Right: positive protrusion with 1 and 2 mm diameter at 1 bar (Nishijima (1992) [38]).

A comparison of various breakdown criteria with measured values of breakdown voltages for sphere-plane and symmetrical sphere-sphere air gaps is given by Donohoe (1998) [39], and shown in Figure 12.

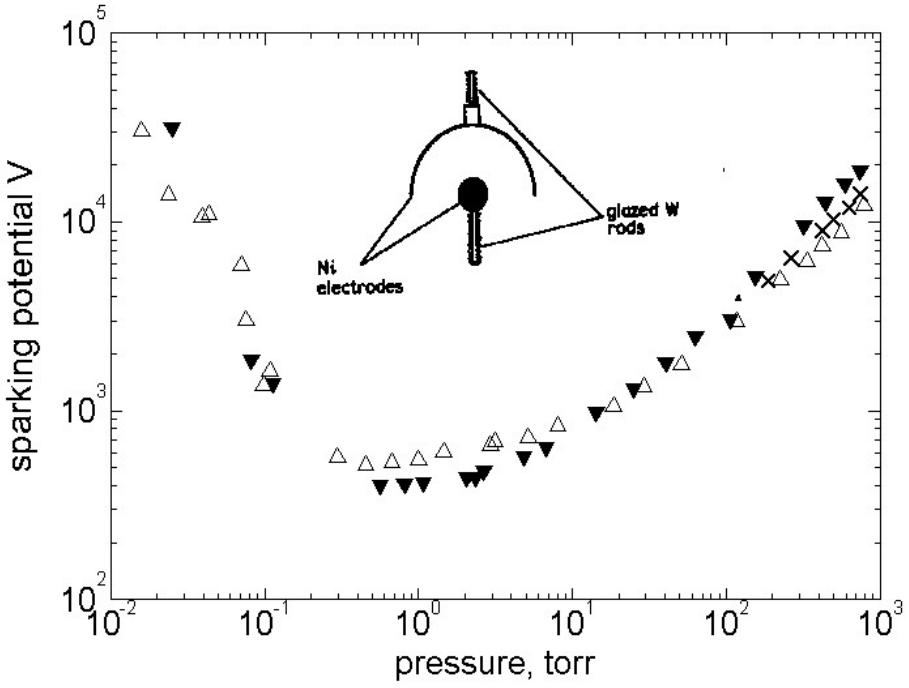

Figure 10. Corona inception and breakdown voltages as function of pressure in dry air for concentric spheres (4.56 mm and 26.5 mm radius, nickel)

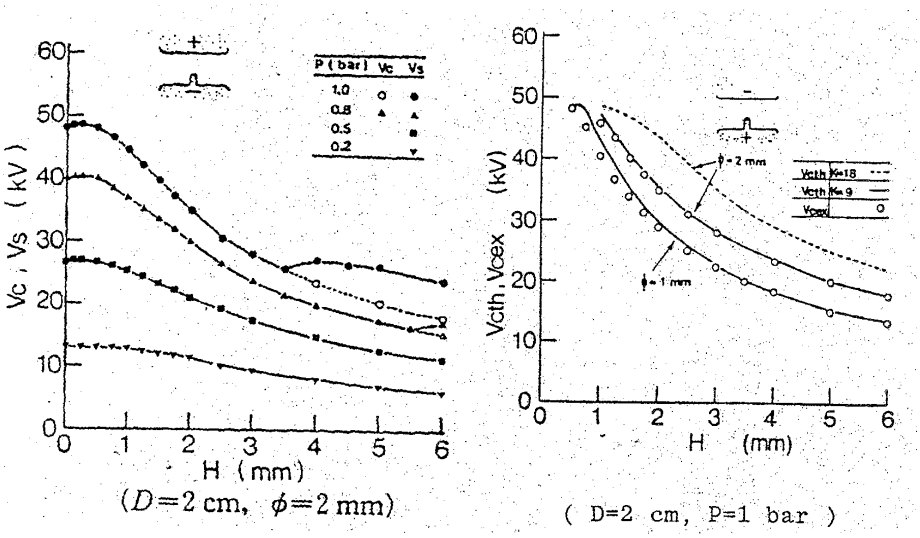

Figure 11. Corona inception and breakdown voltages for gap distance of 2 cm in dry air as a function of protrusion height

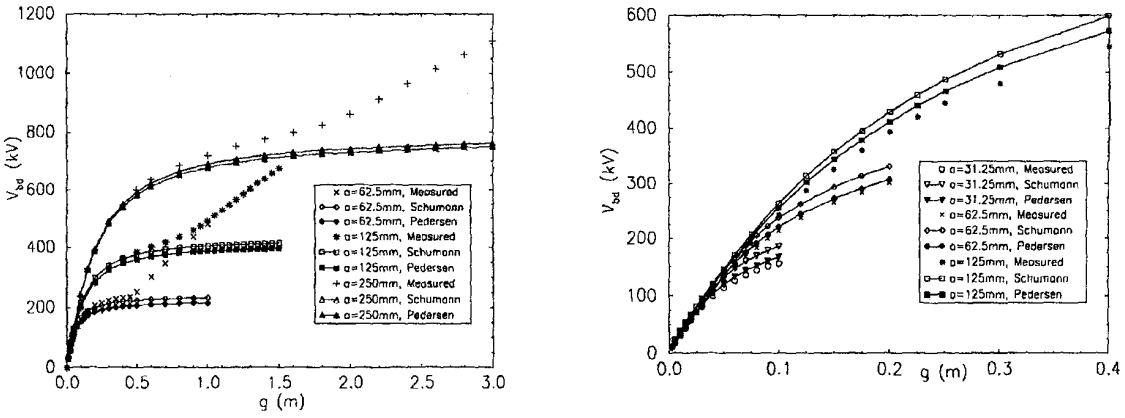

Figure 12. Comparison of different breakdown criteria with measured values of the breakdown voltage for sphere-plane gaps (left) and symmetrical sphere-sphere gaps in air as a function of gap length

3.2.4 Humidity

Several authors investigated the influence of humidity on breakdown in atmospheric air, indicating an increase in breakdown voltage with increasing humidity on the order of 0.2 percent/(g m^{-3}) at a gap distance of 2 cm, and 0.1 percent/(g m^{-3}) at 20 cm (Daeke (1965) [40]; Blair (1963) [41]; and Schroeder (1961) [42]). Physical reasons for the increase are due to attachment of electrons to water molecules (Raju (1973) [36]), and increased ultraviolet (UV) absorption (Schmid (1992) [43]). Raju (1973) [36] reports furthermore on the measurement of breakdown voltages in a sphere (radius 4.56 mm)/hemisphere (radius 26.5 mm) configuration, as a function of pressure (see Table 1).

Table 1. Sparking potentials (in kV) in humid air.

Partial-water-vapour pressure	Total pressure, torr 150	300	450	600	740
torr	kV	kV	kV	kV	kV
0	3·72	6·0	8·10	10·0	12·26
2·5	4·40	6·55	8·70	—	12·4
5·0	4·66	6·90	8·77	10·6	12·6
9·0	4·81	8·0	—	10·7	12·8
12·0	5·0	8·70	8·81	10·8	—
16·0	5·24	8·72	9·60	10·9	12·8

Schmid (1991) [44] and Schmid (1992) [43] reports on increases of the breakdown voltage in humid air of 1.1 percent/(g m^{-3}) at a gap distance of 20 cm for pulsed voltages of 100/6000 ns, with similar results for standard lightning (1.2/50 μs) and switching (60/2000 ns) impulses. (In the notation t_r/t_f, t_r designates the 10 to 90 % risetime to peak amplitude of a double exponential pulse, and t_f is the falltime to half of the peak value.)

4. UNIPOLAR PULSED DISCHARGES

For pulsed discharges, voltages which are higher than the static breakdown voltage for a specific geometry/gas pressure are necessary. For these conditions, i.e., overvoltage, developing avalanches reach charge densities which create electric fields comparable in amplitude to the applied field. Main charge amplification occurs then in the avalanche head, where the electrons have further propagated in the direction antiparallel to the applied electric field than the heavier ions. The usual breakdown criterion for this streamer mechanism is electric field due to space charges > applied electric field. For standard conditions, this happens at charge numbers on the order of 10^8 or αd values (ionizations per unit length times gap distance) on the order of 20 (Raether (1939) [45]; Raether(1940) [46]; Raether (1964) [47]; and Loeb (1940) [48]). The ensuing breakdown mechanism, where generation of photons due to high-energy electron collisions with gas atoms, and subsequent photoionization contribute appreciably to the overall ionization, develops much faster than a discharge following the Townsend mechanism. Average ionization front velocities can reach up to several 10^9 cm/s, with corresponding gap closure times down to several nanoseconds. For practical applications, the question "What pulse duration leads to a discharge for given gap, geometry, gas pressure," replaces the question "What voltage leads to breakdown, for slowly increased voltages, with a Townsend discharge mechanism"?

Figure 13 shows schematically a qualitative picture on streamer development, from Nasser (1971) [8]. In Figure 13, the numbers indicate the following elements: 1. Positive space charge of avalanche, 2. Negative space charge of avalanche, 3. Photons emitted from avalanche, 4. Photoelectrons, 5. Auxiliary avalanches produced by photoelectrons, 6. Streamer tip, 7. Propagating streamer tip by the avalanches feeding into it, 8. Completed streamer channel with some branches.

Much work has been done after Raether to clarify and to quantify the streamer mechanism (see, e.g., Kunhardt 1990) [11]. Main tools have been computer simulations, either finite difference schemes using the basic hydrodynamic (Kline (1972) [49]; Siambis (1971) [50]; and Kline (1974) [51]) or kinetic equations, or particle in cell codes and some analytical work, such as Zakharov (1973) [52]. Examples for experimental verifications of the streamer model include Wagner (1962) [53], (1966) [54], and (1967) [55], Cavenor (1970) [56], Chalmers (1972) [57], and Allen (2001) [58]. Allen reports about repetitive streamer pulses developing from positive corona discharges in gaps of widths of up to 1 m, at voltages in the 400 to 500 kV range, with currents up to milliamperes, and repetition rates of up to 10^5/s. Experimental verifications of breakdown criteria based on the streamer mechanism are reported by Mattingley (1972) [59] and Zaengl (1994) [60] as an effective tool to predict partial discharge inception voltages for curved electrodes.

The classical paper for reports on the measurement of breakdown voltages and breakdown delays for pulsed applied voltages is Felsenthal (1965) [61]. In Figure 14, τ is the formative time. It compares theory and experiment for breakdown in gases, following the sudden application of a dc electric field.

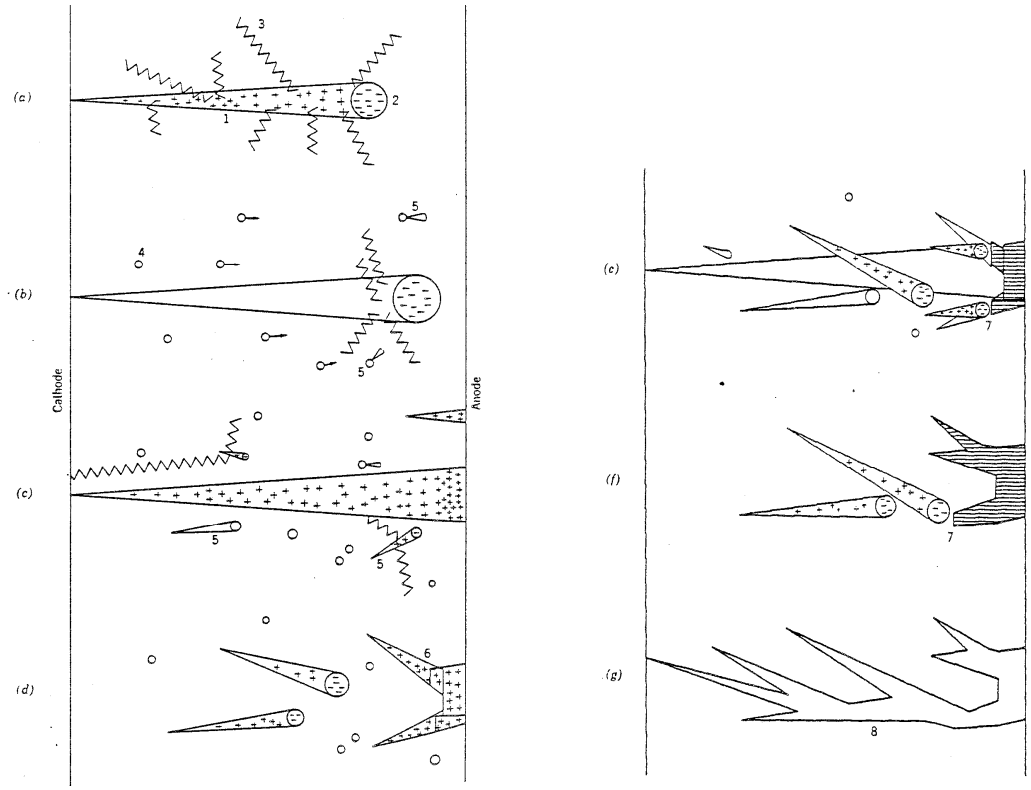

Figure 13. Development of an avalanche into a streamer in a homogeneous field

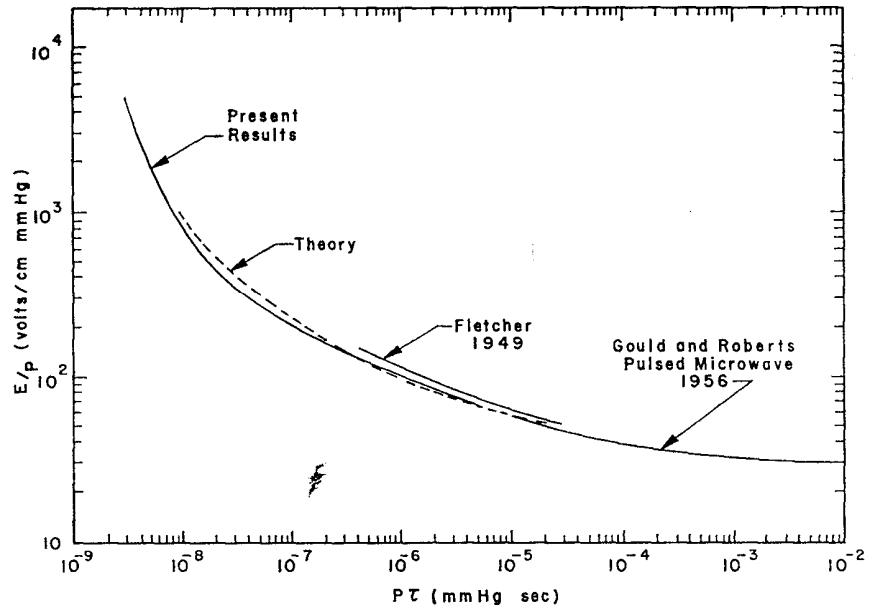

Figure 14. E/p as a function of pτ

Felsenthal's experiments in air cover the parameter range 5 to 30 kV breakdown voltage, 1 to 760 torr pressure, 0.13 to 6 cm gap width, and 0.5 to 18 ns formative time. The

formative time is defined to be the characteristic time for buildup of the ionization in the gap. The curve labeled theory in Figure 14 uses the following equation:

$$P\tau = \frac{\ln(\frac{n_b}{n_0})}{k(\frac{E}{P})(\frac{\alpha}{P} - \frac{\beta}{P})} \quad , \tag{22}$$

where P = pressure, E = electric field, k(E/P) = drift velocity, α = Townsend's first ionization coefficient, β = attachment coefficient, and n_b/n_0 = ratio of breakdown electron density to initial density. Values for k, α, and β are taken from Nielson (1937) [62] and Townsend (1925) [63] for the E/P range of 0.5 to 100 V/cm torr. It seems remarkable that the model used by Felsenthal yields an excellent agreement with experimental data, despite the fact that it is purely based on the Townsend mechanism. The equation above is equivalent to the following:

$$\frac{\partial n}{\partial t} = (\alpha - \beta)kn \quad , \tag{23}$$

Obviously, the dynamics of the streamer process is much faster, and associated time constants can be neglected. Furthermore, the authors claim applicability of this model to pulsed microwave breakdown as well (Gould (1956) [64]). Martin (1985) [65] describes a general semi-empirical model for pulse charged gas gaps with emphasis on SF_6, but he claims the applicability of this model for other gases as well. It is based on negative streamer development, which starts when the electric field on either electrode reaches the dc breakdown value. The negative streamer is considered the sole mechanism which leads to gap closing, even if preceded by a positive streamer.

A direct comparison of pulse charged and dc breakdown in air is given by Molen (1988) [66]. Applied voltage rise was about 20 kV/μs (see Figure 15) A similar behavior for shorter risetime pulses has been shown by Kawada (1988) [67], and is shown in Figure 16. In Figure 16 the impulse waveform, "Thw", is 10.8/74 ns, "Ths" is 10.8/30 ns, and "Vs" is dc (Kawada (1988) [67]).

Most of the experiments with nanosecond pulses have been done at pressures in excess of several 10 bar, which is not too relevant for aerospace conditions. Carboni (2001) [68] reports breakdown fields on the order of 1 to 2 MV/cm for stress times (duration of applied voltage) of 1 to 5 ns in air (gap width 0.091 cm, pressure 30 to 100 bar). Measured minimum risetimes in H_2 are on the order of 200 to 300 ps. Mankowski (1998) [69] reports similar results: breakdown times down to 0.5 ns at field amplitudes of around 0.8 MV/cm with positive point electrode (25 μm radius) and around 1.3 MV/cm with negative tip, at 400 psi in air. With hemispherical electrodes (diameter 2 cm) breakdown times of 0.5 ns are observed at 2 MV/cm at 400 psi.

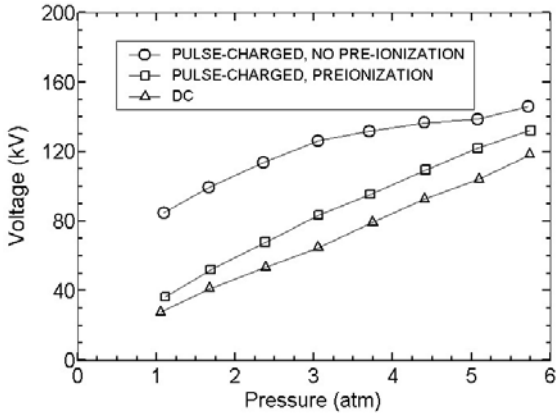

Figure 15. Comparison of pulse-charged (20 kV/μs) and dc charged breakdown voltages, gap distance 1 cm, rod electrodes with 0.95 cm diameter and hemispherical tip, as a function of pressure

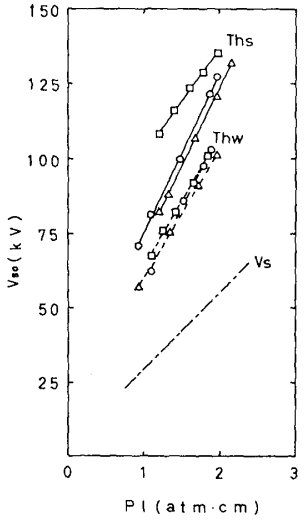

Figure 16. A comparison of dc and impulse breakdown voltages in air versus pd, where Thw is for 10.8/74 ns, Ths is for 10.8/30 ns, and V_S is for dc.

With smaller curvature electrodes, breakdown delay times in the subnanosecond regime can be reached with applied voltages of less than 10 kV (see Figure 17 as an example from Krompholz (2001) [70]. In Figure 17, the cathode radius is 0.5 μm, gap width is 1 mm.

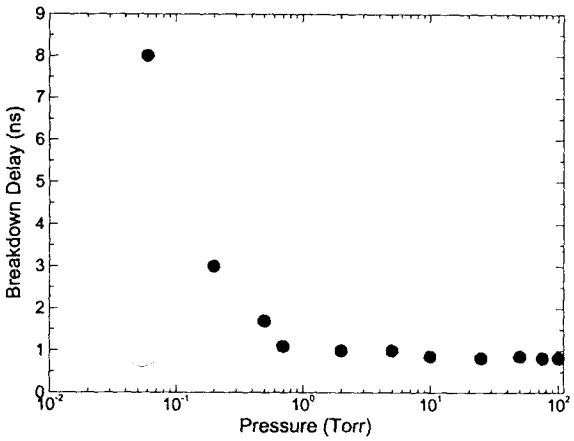

Figure 17. Breakdown delay time in argon as a function of pressure for an applied voltage amplitude of 14 kV

5. HIGH FREQUENCY AC BREAKDOWN

For homogeneous fields, two characteristic frequencies, one for ions, f_{ci}, and one for electrons, f_{ce}, are important. The quantity f_{ci} is the frequency for which positive ions are no longer able to drift out of the gap before voltage reversal, as defined by

$$d = \frac{k^+ E_0}{\pi f_{ci}} \quad , \tag{24}$$

where k^+ is the ion mobility, E_0 the dc breakdown field, and d the gap distance. For frequencies below f_{ci}, the breakdown mechanism is basically the same as for dc; for $f > f_{ci}$, ions may accumulate in the gap, and cumulative space charge effects play a major role, usually lowering the breakdown voltage. Figure 18 shows a typical example for this behavior, breakdown voltages in atmospheric air as a function of gap distance, for 50 Hz (which is essentially identical to dc), 0.5 and 1 MHz (Misere (1932) [71].

Other authors (e.g., Mueller (1934) [72]) report a critical gap length below which the breakdown voltage is independent of the frequency, the critical gap length increasing with decreasing frequency, i.e., 0.45 cm at 110 kHz and 0.09 cm at 995 kHz (Meek, 1978, pg. 690 [7]). Consideration of positive ion mobilities show that these critical gap lengths correspond roughly to those for which accumulation of positive ions is expected to occur in the gap. (See Figures 19 and Figure 20 from Nasser, 1971 [8]). In Figure 20, curve 1: 110 kHz, Curve 2: 140 kHz, Curve 3: 310 kHz, Curve 4: 880 kHz, Curve 5: 1450 kHz (Nasser, 1971, pg. 369 [8]). The rise in breakdown voltage for higher frequencies, as shown in Figure 20, for $f > 3$ MHz is due to the start of electron oscillations in the gap which reduce the effect of the positive ion space charge.

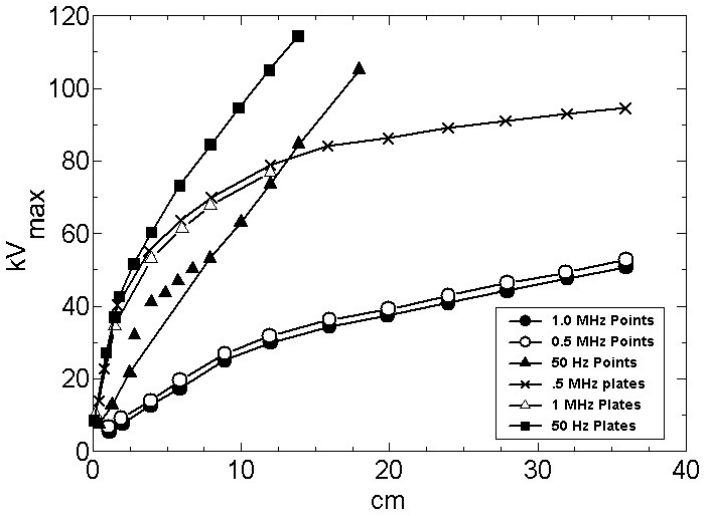

Figure 18. Reduction of breakdown voltage in atmospheric air as a function of gap distance, for 50 Hz, 0.5 MHz, and 1 MHz.

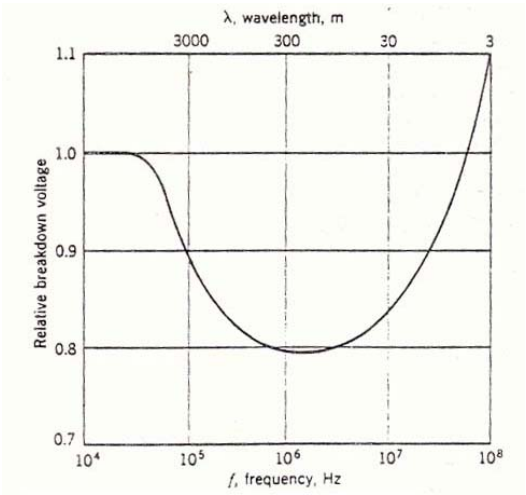

Figure 19. Breakdown voltage as a function of frequency for a 1-cm uniform field gap in atmosphere air

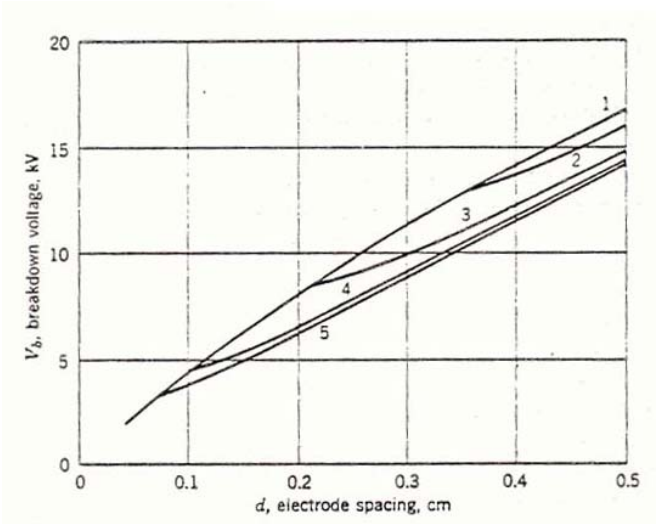

Figure 20. Breakdown voltage between two large spheres in atmospheric air, as a function of gap distance for different frequencies;
Curve 1: 110 kHz, Curve 2: 140 kHz, Curve 3: 310 kHz,
Curve 4: 880 kHz, Curve 5: 1450 kHz

A similar frequency to f_{ci} for ions, f_{ce}, can be defined for electrons, which describes the limit between mobility controlled breakdown ($f < f_{ce}$, electrons are lost to the electrodes due to their mobility) and diffusion controlled breakdown (for $f > f_{ce}$, electrons are not able to drift to the electrodes during one half-cycle, but might be lost from the volume filled with critical field by diffusion). As a consequence, breakdown voltages for frequencies below f_{ci} are essentially the same as dc breakdown voltages. For frequencies between f_{ci} and f_{ce}, ion space charge will oscillate between the electrodes, which facilitates the growth of new avalanches and lowers the breakdown voltage below dc levels. For frequencies above f_{ce}, ionization by electrons is reduced since a large fraction of the electron distribution is no longer subject to the adequately accelerating fields, and the breakdown voltage is increased as compared to dc.

Figure 21 shows typical breakdown voltages in atmospheric air, as a function of gap length from 0 to 0.8 mm, for frequencies between 100 and 300 MHz (Pim (1949) [73]). The discontinuities represent the critical gap length ($d \sim 1/f_{ci}$) below which the breakdown voltage is approximately the same as for dc (slightly lower). At longer gap lengths, the voltage is reduced by up to 40 percent as compared to dc, which the authors relate to oscillating electron avalanches confined to the gap, a process similar to a multipactor mechanism for free electrons, supported by the presence of positive ions in the gap. (Multipactor is a mechanism that occurs when electrons accelerated by radio-frequency fields create a self-sustaining discharge under low pressures, via an electron avalanche caused by secondary electron emission from surfaces.) Figure 22 (Pim (1949) [73]) shows breakdown voltage versus gap length as a function of pressure, with a strong reduction of breakdown voltage at low pressures.

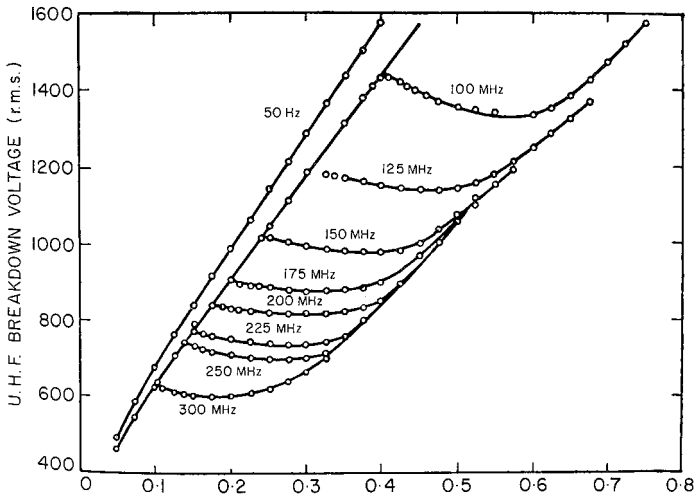

Figure 21. Breakdown voltage as a function of gap distance in cm for atmospheric air

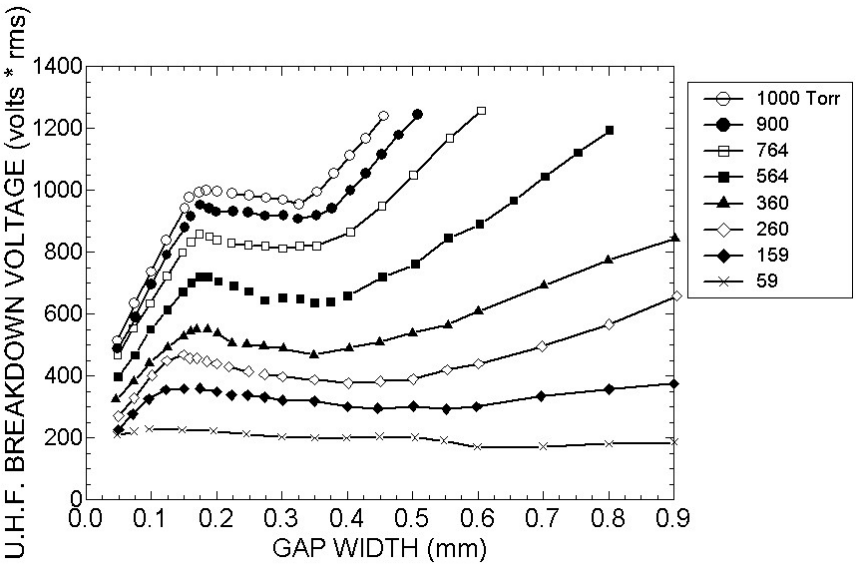

Figure 22. Breakdown voltage between parallel plates in atmospheric air as a function of gap distance at different pressures

For frequencies extending into the microwave regime, diffusion controlled breakdown takes over. The classical ac breakdown model describes this regime, where only the average electron motion is considered, based on

$$m\frac{dv}{dt} = -eE - m\nu_m v \quad , \tag{25}$$

where v is the average electron velocity, and ν_m the collision frequency for momentum transfer. As a result (see, e.g., Nasser (1971) pp. 379 - 380) [8]), the breakdown field is calculated as follows:

$$E_b = \nu_m(m^3v^2/eM)^{1/2} \quad \text{for} \quad \nu_m > \varpi \; ; \quad E_b = (\varpi/\Lambda\nu_m)(mv^2W_i/3e)^{1/2} \quad \text{for} \quad \nu_m < \varpi, \qquad (26)$$

where $\Lambda = (D/\nu_i)^{1/2}$, is the diffusion length, and W_i the ionization energy.

The breakdown voltage versus pressure then has a minimum at the value which corresponds to $\nu_m = \varpi$; designated by a linear fall below and a linear rise (on a log/log scale) above this value from calculations (See Figure 23 from Nasser (1971) pg. 381 [8]; also Brown (1966) [74].) In Figure 23, the specific numbers are for helium with a small admixture of mercury vapor.

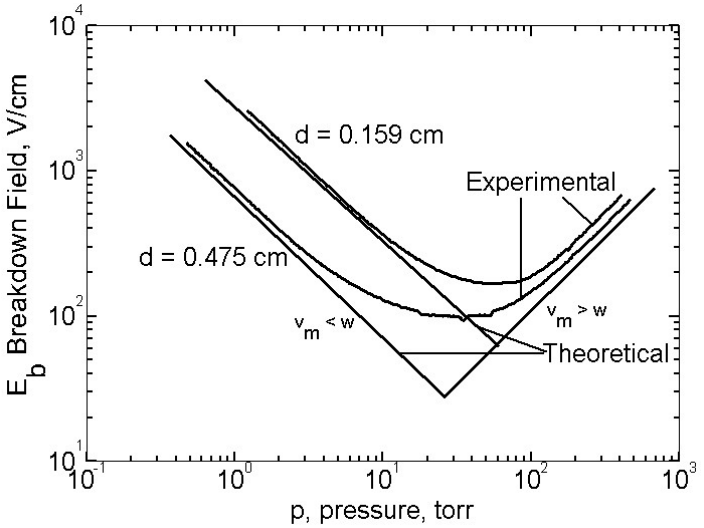

Figure 23. A comparison of breakdown field vs. pressure for the microwave regime.

Actual results of measurements confirm this behavior, (see, e.g., Figure 24, Meek (1978) pg. 707 [7], Herlin (1948) [75] and Figure 25, MacDonald (1966) [76]). In Figure 24, cavity lengths range between 0.0635 and 7.62 cm.

For pulsed conditions, we expect the breakdown field is expected to increase as compared to CW sinusoidal ac conditions. Some measurements from the 1960s for pulse width from about 30 ns to the microsecond regime, see Figure 26 (Gould (1956) [64]), and Figure 27 (MacDonald (1966) [76]). In Figure 26, data are for pressures near the minima of CW breakdown fields.

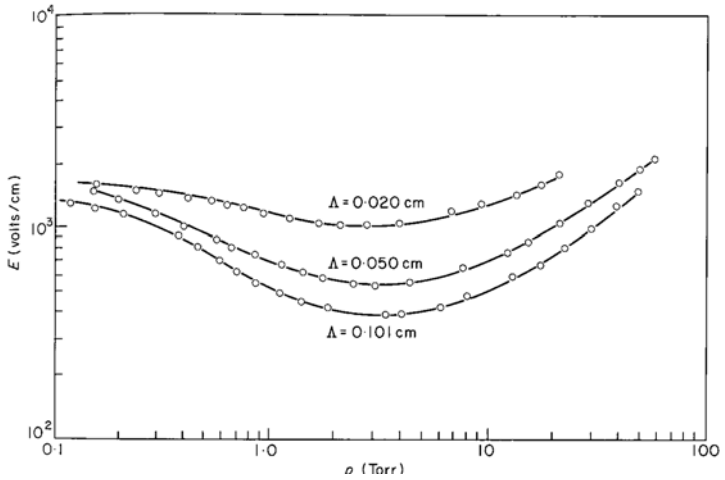

Figure 24. The CW breakdown field as function of pressure for 3.13 GHz.

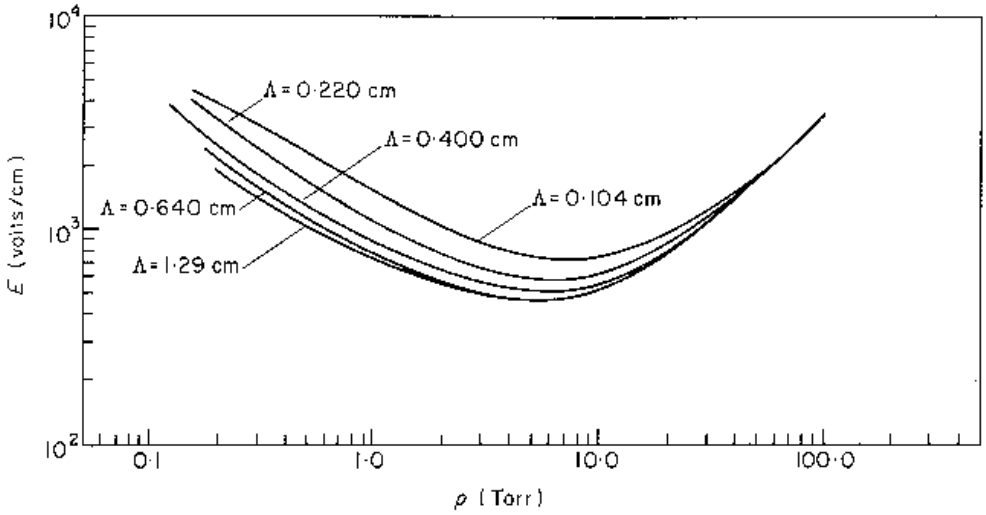

Figure 25. The CW breakdown fields in air as a function of pressure for 9.4 GHz

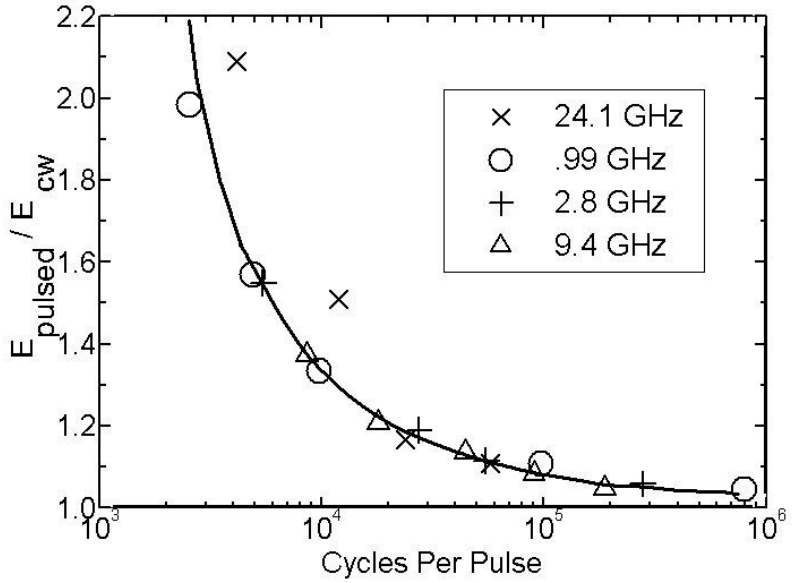

Figure 26. Ratio of breakdown field for pulsed microwaves to that microwaves

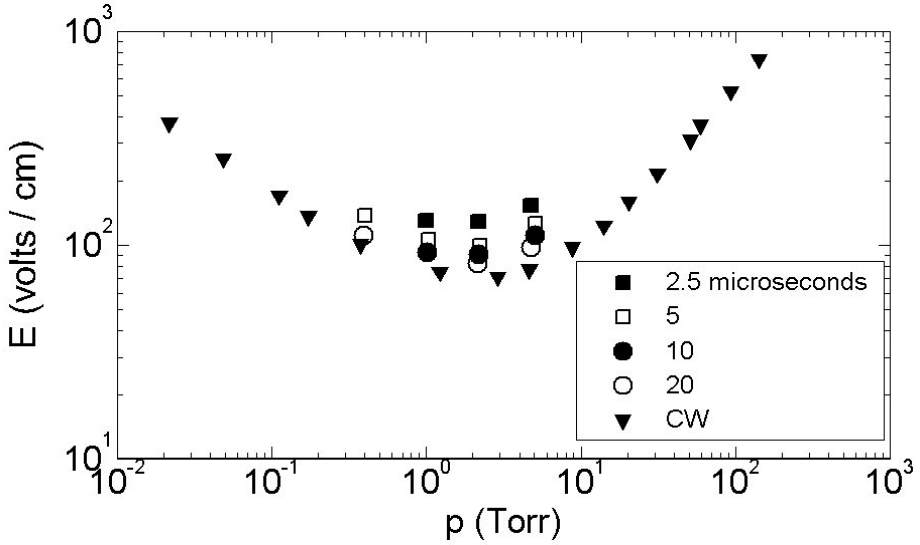

Figure 27. Breakdown fields for pulsed and CW microwaves (at 994 MHz in air); gap = 1.51 cm, repetition rate 1 kHz

The increased use of power semiconductors in power conditioning equipment has resulted in high electric field stresses at high frequencies in electronic equipment. Pfeiffer (1991) [77] reported on experimental investigations at frequencies to 100 kHz for various electrode geometries in air: uniform and non-uniform fields, surface flashover and partial discharge.

More recent work on microwave breakdown has been done in connection to the high power microwave Multidisciplinary University Research Initiative (MURI) program funded by the Air Force Office of Scientific Research (AFOSR) from 1995 to 2000

(Neuber (1999) [78], and Neuber (2001) [79]), where all major aspects of pulsed breakdown, such as multipactor in waveguides and cavities, and breakdown in gases and along microwave windows, have been covered. Susceptibility curves (voltage range for which two-sided multipactor is possible) were studied by Kishek (1988) [80]. Breakdown fields on the vacuum side of windows start with field values on the order of 10 kV/cm. Also, the influence of background gas on surface flashover, as well as volume breakdown, has been investigated by Hemmert (2000) [81]. (See Figures 28 through Figure 30 by Hemmert (2002) [82].) The experiments reported here use field enhancement points (copper triangles with a radius of curvature of 1 mm) forcing a discharge along the electric field in an S-band waveguide.

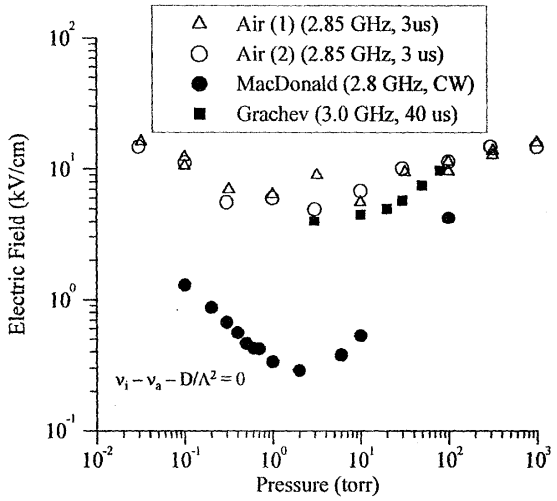

Figure 28. Breakdown field for pulsed and CW microwaves in air

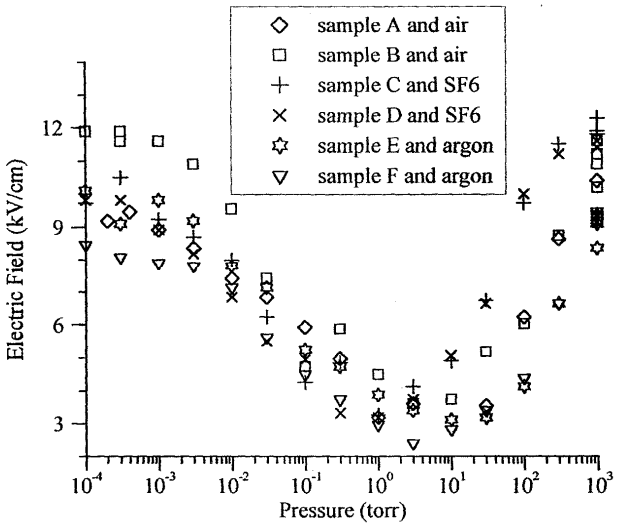

Figure 29. Breakdown field at gas/alumina interface for 2.85 GHz

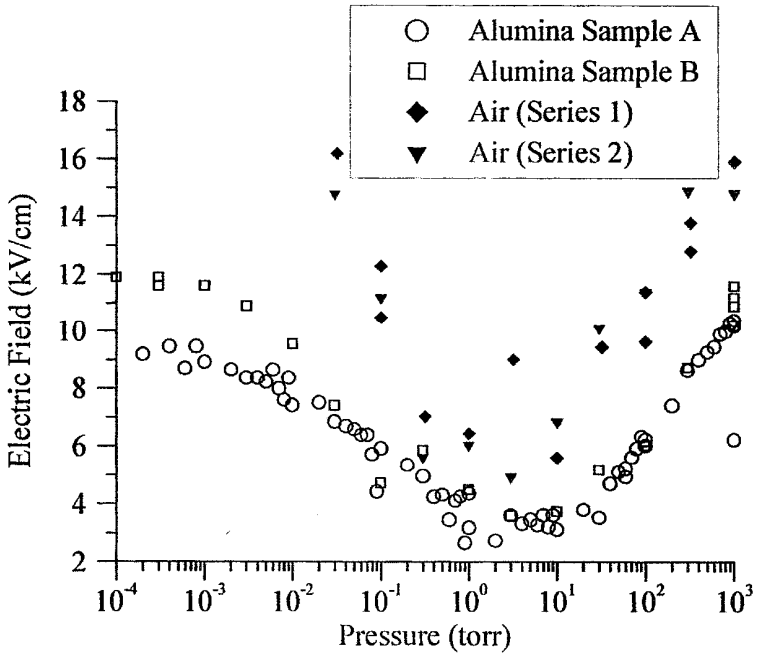

Figure 30. Comparison of breakdown field along the surface of alumina and volume discharge

Breakdown work has been done at frequencies related to switching applications for power conditioning equipment, in partial vacuum (high altitude) environments. Experimental investigations were conducted on the breakdown characteristics of helium, nitrogen and zero air under unipolar sinusoidal and pulsed voltages at frequencies varying from 20 kHz to 220 kHz in partial vacuum, for point-to-point and point-to-plane electrode configurations. Breakdown voltages were also compared to dc data obtained under similar conditions (Koppisetty, 2008 [83]).

6. SUMMARY

The information in this report is meant as a guide to the development of electrical insulation design strategies for advanced airborne power systems. It is a compilation of parametric guidelines, gathered through a literature search that can be used by power system designers, though it is not a designer's guide, by any means. The following is a summary of this information, including additional work that should be performed to broaden the range of useful parametric data.

High-voltage gas electrical breakdown characteristics have been studied over a fairly wide range of parameters; however, the potential parameter space is even larger. The earliest work involved the most straightforward conditions and covered simple, uniform dc electrical fields. From sea level to ~ 100,000 feet, the breakdown process is dominated by gas collisional processes and is, to first order, proportional to the product of the pressure

(p) and the electrode spacing (d). Paschen theory was summed up earlier by the following equation for the breakdown voltage:

$$V_B = \frac{Bpd}{\ln\{\frac{Apd}{\ln(1+\frac{1}{\gamma_i})}\}} \quad , \tag{27}$$

where A, B, and γ_i were characteristics of the particular gas. This relationship has been experimentally verified for a wide range of pressures, distances, and gases; and was shown earlier in Figure 3. For nonuniform fields, breakdown will be enhanced for electrodes with small radii of curvature as shown in Figure 8. Note that electrical breakdown with curved electrodes does not vary much from the flat plate case until the radius of curvature falls below one centimeter. Finally, relative humidity has very little effect (< 0.2 percent) on breakdown up through 100 percent saturation. Electrode materials can also influence breakdown voltages; however, in most cases the effect is less than 10 percent. Electrode conditioning can introduce factors of two or more (see Figure 6), and special treatments (or mistreatments) can further enhance this situation. These effects are much more idiosyncratic, and each situation must, therefore, be assessed on a case-by-case basis. For low pressures (< 10^{-3} torr), corresponding to very high altitudes or the near-earth space environment, gas collisions become much less important and dc breakdown behavior transitions from gas-dominated processes to pure vacuum discharge. In this case, electrode materials and conditioning totally dominate the picture, and discharge thresholds must either be individually (experimentally) characterized, or very large safety factors must be included to avoid inadvertent breakdown.

Pulsed dc discharge generally occurs at somewhat higher voltages than continuous dc because actual breakdown must be preceded by streamer formation. This phenomenon becomes increasingly important as either the pressure (p) or formative time (τ) is reduced (evidenced by Figure 14).

The microwave breakdown regime is the most complex since, depending on the frequency and gap spacing, the electrons may or may not have sufficient time to initiate an avalanche breakdown. This, in turn, depends on the electron and ion collision times (mobilities) that are a function of pressure. Although this area has been researched extensively, the literature search only spans a fraction of the possible variables. To be complete, the experimental parameter space ideally needs to span the parameter ranges shown in Table 2.

There is a huge parameter space for gas discharge initiation. This report has emphasized conditions relating to high voltage applications in aerospace environments. Breakdown numbers have been found by this literature search for a pressure regime of ~ 10^{-4} to one Bar for air, for a variety of the parameters in Table 2. Figure 31 depicts where some of this data falls on a pressure versus gap width plot for a variety of frequencies and pulse lengths for air. For instance, the dotted rectangle represents the 3 GHz work performed by Herlin [75]. The diagonals represent constant voltages on a Paschen diagram, where the lower 1 kV line corresponds to the left hand side (for small pd) of the Paschen curve.

Table 2. Microwave breakdown desirable parameter space

Parameter	Range
Pressure	Sea level (~ 1 Bar) to near earth space (~ 10^{-6} Bar)
Gap width	~ tenth of a millimeter to ~ one meter
Frequency	dc to ~ 10 GHz
Pulse length	~ 10^{-9} sec (ns) to ~ 10^{-3} sec (ms)
Electrode curvature	Flat to ~ one millimeter
Electrode materials	Copper, stainless steel, aluminum, etc.
Electrode conditioning	Untreated, chemically cleaned, electropolishing, etc.
Gases	Air, N_2, O_2, CO_2, Ar, He, H_2, …

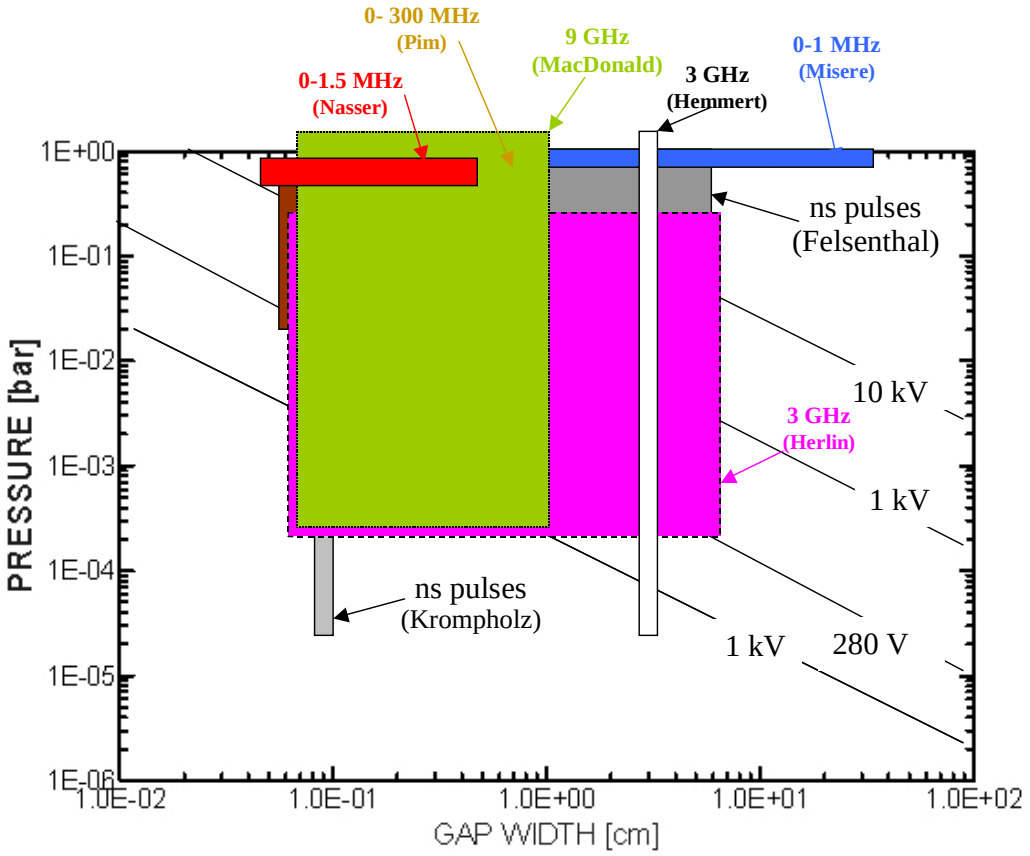

Figure 31. Areas covered in p versus d space by most relevant publications

Figure 31 does not completely span the desired parameter space. Even though gas breakdown characteristics have been studied over a fairly wide range of parameters, the parameter space has been somewhat defined by the needs of commercial equipment design. In the study of gas environments, volume breakdown caused by dc voltages is

well documented. However, for many conditions of other applied voltage waveforms, huge gaps in the environmental parameter space still have to be explored. Breakdown caused by nanosecond and sub-nanosecond pulses, under special conditions at pressures of one atmosphere and below, has been investigated, but not in depth. This regime gains more and more importance due to new developments, such as ultra-wideband radar. The applicability of repetition-rated, short high voltage pulses to metallic structures (such as wire antennas) is lacking information in the literature. Another information gap appears in the initiation of discharges along surfaces. While significant research has been done on flashover in vacuum, surface flashover along insulators in a partial-vacuum (sub-atmospheric pressure) gas environment has been minimal. This is extremely important for the design of feedthroughs and bushings in power conditioning equipment that must operate at very high altitudes. For sinusoidal ac breakdown, there are excellent models describing the breakdown phenomena. However, for pulsed conditions (and especially short pulses) not much information exists for breakdown in waveguides and cavities, in open space, and along window interfaces. Likewise, repetitively pulsed gas and surface breakdown under partial vacuum, high altitude conditions has not been fully investigated. This is particularly relevant for pulse-width-modulated (PWM) drives for rotating machinery, e.g., electrical actuators for advanced aircraft.

7. REFERENCES

1. Paschen, F. (1898), Wied. Ann., **37**, 69

2. de la Rue, W., and Mueller, H.W. (1880), *Phil. Trans. Roy. Soc*., **171**, 109.

3. Hurst, H.E. (1906). *Phil. Mag*., **11**, pg. 535

4. Townsend, J.S. (1900) *Nature*, **62**.

5. Townsend, J.S. (1901) *Phil. Mag*. **198** 340.

6. Townsend, J.S. (1902) *Phil. Mag*. **6**.

7. Meek, J.M., and Craggs, J.D. (1978), *Electrical Breakdown of Gases*, Wiley-Interscience.

8. Nasser, E. (1971), *Fundamentals of Gaseous Ionization and Plasma Electronics*, Wiley, New York.

9. Novak, J.P., and Bartnikas, R. (1987), *J. Appl. Phys*. **62**, 3605.

10. Pedersen, A. (1989), "On the electrical breakdown of gaseous dielectrics," *IEEE Transactions on Electrical Insulation* **24**, 721.

11. Kunhardt, E.E. (1990), "Electrical breakdown in gases in electric fields", in *Gas Discharge closing switches*, G. Schaefer ed., Plenum Press, New York

12. Kunhardt, E.E., and Byszewski, W.W., 1980, "Development of overvolted breakdown in high pressure gases," *Phys. Rev. A*, **21**, 2069.

13. Dutton, J., Llewellyn Jones, F., and Palmer, R.W., (1961), Proc. Phys. Soc. **78**, 569. See also MC Figure 3.11, page 229.

14. Allen, N.L., Lam, S.K., and Greaves, D.A. (2000), "Tests on the breakdown of air at elevated temperatures in non-uniform electric fields," *IEEE Proc.-Sci. Meas. Technol*. **147**, 291.

15. Hanlon, J.T., 1974, "Paschen breakdown measurement techniques for dry Reed capsules and relays," Proc. 3rd Int'l annual National Relay Conference, Stillwater, OK, pg. 15-1.

16. George, D.W. (1974), "Electrical breakdown in variable density gases," Proc. 3rd Int'l Conf. on Gas Discharges, London, England, pg. 127.

17. Powell, C.W., and Ryan, H.M. (1972), "Breakdown characteristics of air at high temperature," 2nd Int'l. Conf. on Gas Discharges, *IEE Conf. Publication* 50, pg. 285.

18. Hiziroglu, H.R., and Sebo, S.A. (2000), "Calculation of breakdown voltages of short air gaps," 2000 Conference on Electrical Insulation and Dielectric Phenomena, Victoria, Canada, IEEE Cat. Nr. CH37132, pg. 435.

19. Geballe, R., Harrison, M.A. (1952), *Phys. Rev*. **85**, 372.

20. Schoenhuber, M.J. (1969), "Breakdown of gases below Paschen minimum: Basic design data of high-voltage equipment," *IEEE Transactions on Power apparatus and Systems*, Vol. **PAS-88**, 100.

21. Hackam, R, and Raju, G. (1974), "Electrical breakdown of a point-plane gap in high vacuum and with variation of pressure in the range $10^{-7} – 10^{-2}$ Torr of air, nitrogen, helium. sulphur hexafluoride, and argon," *Journal of Applied Physics*, **Vol. 45, No.11**, 4784.

22. Bhasanavich, D., and Parker, A.B. (1977), "The dielectric breakdown of gases at low pressure," *Proc. R. Soc. Lond.* **A 358**, 385.

23. Lisovskiy, V.A., Yakovin, S.D., and Yegorenkov, V.D. (2000),"Low-pressure gas breakdown in uniform dc electric field," *J. Phys. D: Appl. Phys* **33**, 2722.

24. Watson, P.K., and Sharbaugh, A.H. (1969), "The electric strength of nitrogen at elevated pressures and small gap spacings," *J. Appl. Phys* **40**, 328.

25. Goldspink, G.F., and Lewis, T.J. (1968), "Erratic gas breakdown at high pressures," Proc. Conf. on Electrical Insulation and Dielectric Phenomena, pg. 101.

26. Coates, R., Dutton, J., Harris, F.M. (1974), "The role of the electrode surface in the breakdown of gases in high uniform fields," Proc. 3rd Int'l Conf. on Gas Discharges, London 1974, pg. 403.

27. Ramirez, J.J. (1976), "Effect of electrode surface conditions on the self-breakdown strength and jitter of a high-pressure pulse gas switch," *J. Appl. Phys* **47**, 1925.

28. Cookson, A.H. (1970), Proc. IEE, **117**, 260.

29. Cookson, A.H. (1981), "Review of high-voltage gas breakdown and insulators in compressed gas," IEE Proc. **128**, 303.

30. Llewellyn Jones, F. (1939), *Phil. Mag*. **28**, 192.

31. Morokuma, Y., Nakamura, Y., and Mori, T. (1969), "The influence of cathode surface state on Townsend discharge in argon," Proc. Int'l Conf. on Phenomena in ionized gases, Bucharest, Pg. 113.

32. Mahdy, A.M., Anis, H.I., and Ward, S.A. (1998), "Electrode roughness effects on the breakdown of air-insulated apparatus," *IEEE Transactions on Dielectrics and Electrical Insulation*, **5**, 612.

33. Engel, A. (1993), *Ionized Gases*, Reprint American Vacuum Society Classics, ISBN 1-56396-272-1, AIP Press (Original 1955, Oxford University Press).

34. Mesyats, G.A. (2004), *Pulsed Power*, Plenum Press, New York.

35. Werner, S. (1934), "Types of discharges in cylindrical tube counters," *Z. Phys*. **90**, 384.

36. Raju, G., and Hackam, R. (1973), "Sparking potentials of dry air, humid air and water vapor between concentric sphere-hemisphere electrodes," *Proc. IEE* **120**, 927

37. Barsch, J.A., Sebo, S.A., and Kolcio, N. (1992), "Power frequency ac sparkover voltage measurements of small air gaps," *IEEE Transactions on Power Delivery*, **14**, 1096.

38. Nishijima, K., and Tsuneyasu, I. (1992), "Comparisons of direct-current breakdown characteristics in dry air and SF6 gaps using a parallel-plane arrangement with variable height protrusion," Electrical Engineering in Japan, **112**, 46.

39. Donohoe, J.P. (1998), "Physical characteristics of criteria governing the computation of air gap breakdown voltages for slightly divergent fields," *IEEE transactions on dielectrics and electrical insulation* **5**, 485.

40. Daeke, C.U. (1965), Z. angew. Phys. **19**, 453.

41. Blair, D.T., Bruce, F.M., and Tedford, T.J. (1963), Proc. 6th Int'l Conf. on Phenomena in Ionized Gases, Paris, Vol. 1, pg. 321.

42. Schroeder, G.A. (1961) *Z. angew. Phys*. **13**, 296.

43. Schmid, J. (1992), "Influence of absolute humidity on the electrical breakdown in air," *ETEP*, Vol. 2, pg. 327.

44. Schmid, J., and Feser, K. (1991) "Humidity influence on the breakdown voltage of an air gap with fast rising impulse voltages," Proc. 7th Int. Symp. On High Voltage Engineering, Dresden, Germany, paper 42.12, pg. 113.

45. Raether, H. (1939), *Z. Phys*. 112, 464.

46. Raether, H. (1940), *Arch. F. Elektrotech*. **34**, 49.

47. Raether, H. (1964), *Electron Avalanches and Breakdown in Gases*, Butterworths, London.

48. Loeb, L.B., and Meek, J.M. (1940), *J. Appl. Phys*. **11**, 438.

49. Kline, L.E., and Siambis, J.G. (1972), "Computer simulation of electrical breakdown in gases: avalanche and streamer formation," *Phys. Rev*. **A5**, 794.

50. Siambis, J.G., and Kline, L.E. (1971), "A new computer technique for the simulation of electrical breakdown phenomena in gases," AICA Symposium on Simulation of Complex Systems, Tokyo, pg. F10-1

51. Kline, L.E. (1974), "Calculations of discharge initiation in overvolted parallel-plane gaps," *J. Appl. Phys*. **45**, 2046.

52. Zakharov, A.I. *et al.* (1973), "A contribution to the theory of streamer breakdown," *Journal of applied mechanics and technical physics*, **14**, 45

53. Wagner, K.H., and Raether, H. (1962), *Z. Phys*. **170** 540.

54. Wagner, K.H. (1966), *Z. Phys*. **189** 465.

55. Wagner, K.H. (1967), *Z. Phys*. **204** 177.

56. Cavenor, M.C. (1970), "An experimental test of the streamer breakdown criterion," *Aust. J. Phys*. **23**, 953.

57. Chalmers, I.D., Duffy, H., and Tedford, D.J. (1972), "The mechanism of spark breakdown in nitrogen, oxygen, and sulphur hexafluoride," Proc. R. Sc. Lond. A. **329**, 171.

58. Allen, N.L., and Mikropoulos, P.N. (2001), "Surface Profile Effect on Streamer Propagation and Breakdown in Air", IEEE Transactions on dielectrics and Electrical Insulation **8,** 812

59. Mattingley, J.M., and Ryan, H.M. (1971), “Breakdown voltage estimation in air and nitrogen, Conf. on Electrical Insulation and Dielectric Phenomena, Williamsburg VA, pg. 141.

60. Zaengl, W.S., and Petcharaks, K. (1994), “Application of streamer breakdown criterion for inhomogeneous fields in dry air and SF6,” *Gaseous Dielectrics* VII, L.G. Christophorou ed., Plenum Press, New York.

61. Felsenthal, P., and Proud, J.M. (1965),”Nanosecond pulse breakdown in gases,” *Phys. Rev.* **6A**, 1796.

62. Nielson, R.A., and Bradbury, N.E. (1937), Phys. Rev. **51**, 69.

63. Townsend, J.S. (1925), *Motion of electrons in gases*, Clarendon Press Oxford.

64. Gould, L., and Roberts, L.W. (1956) *J. Appl. Phys*. **27**, 1162.

65. Martin, T.H. (1985), Proc. 5th Pulsed Power Conf., Arlington, VA, pg. 74.

66. Molen, G.M., and Mazzola, M.S. (1988) *IEEE Conf. Record of 18th Power Modulator* Hemmert. D., Neuber, A.A., Dickens, J.C., Krompholz, H., Hatfield, L.L., and Kristiansen, M. (2000a), “High power microwave window breakdown under vacuum and atmospheric conditions,” Proc. Of the SPIE, Intense Microwave Pulses VII, Vol. 4031, pg. 90.

67. Kawada, Y., Shamoto, S., and Hosokawa, T. (1988), *J. Appl. Phys*. **63**, 1877.

68. Carboni, V., Lackner, H., Giri, D., and Lehr, J. (2001), “The breakdown fields and risetimes of select gases under the conditions of fast charging (20 and or less) and high pressure (20 to 100 atmospheres)”, Proc. 13th Int. Pulsed Power Conference, pg. 482.

69. Mankowski, J., Dickens, J., and Kristiamsen, M. (1998), “High voltage sub-nanosecond breakdown,” *IEEE Transactions on Plasma Science* **26**, 874.

70. Krompholz, H., Hatfield, L.L., Kristiansen, M., Hemmert, D., Short, B., Mankowski, J., Brown, M., and Altgilbers, L. (2001), “Gas breakdown in the sub-nanosecond regime with voltages below 15 kV,” Proc. IEEE 13th Pulsed Power Conf., pg. 487.

71. Misere, F. (1932), *Arch. Elektrotech.* **26**, 123.

72. Mueller, F. (1934), *Arch. Elektrotech.* **28**, 341.

73. Pim, J.A. (1949), Proc. IEE **96**, Part III, 117.

74. Brown, S.C. (1966), *Introduction to Electrical Discharges in Gases*, Chapter 10, Wiley, New York.

75. Herlin, M.A., and Brown, S.C. (1948), *Phys. Rev*. **54**, pg. 1650.

76. MacDonald, A.D. (1966), *Microwave breakdown in gases*, Wiley, New York

77. Pfeiffer, W. (1991), “High-frequency Voltage Stress of Insulation”, IEEE Transactions on Electrical Insulation, Vol. 26, No. 2, pg. 239

78. Neuber, A., Hemmert, D., Krompholz, H., Hatfield, L., and Kristiansen, M. (1999), “Initiation of high power microwave dielectric interface breakdown,” *J. Appl. Phys*. **86**, 1724.

79. Neuber, A.A., Laurent, L., Lau, Y.Y, and Krompholz, H. (2001), "Windows and rf Breakdown," in *High power microwave sources and technologies*, Barker, R.J., Schamiloglu, E., eds., IEEE Press Series on HF and Microwave Technology, IEEE Press, New York.

80. Kishek, R.A., Lau, Y.Y., Ang, L.K., Valfells, A., Gilgenbach, R.M. (1988), *Phys. Plasmas* **5**, 2110.

81. Hemmert, D., Neuber, A.,., Krompholz, H., Hatfield, and L.L., Kristiansen, M. (2000), "Pressure dependence of high power microwave solid dielectric/gas interface breakdown," Abstracts 27th *IEEE Int. Conf. on Plasma Science*, 124.

82. Hemmert, D. (2002), Ph.D. dissertation, Department of Electrical and Computer Engineering, Texas Tech University, Lubbock, TX.

83. Koppisetty. K, (2008), Ph.D. dissertation, Department of Electrical and Computer Engineering, Auburn University, Auburn, AL.